Two-motor, two-axle traction system for full electric vehicle

Claudio Rossi, Davide Pontara, Marco Bertoldi, Domenico Casadei

Dept. of Electrical, Electronic and Information Engineering "G. Marconi"
University of Bologna – ITALY
First_name.Last_name@unibo.it

Abstract

The paper deals with the description of a low voltage, two-battery pack, two-motor, two-axle powertrain configuration for a full performance compact electric car. It gives an analytical method for selecting the two different drives for front and rear axle, a performance and economical evaluation criteria for choosing the low voltage active components and gives details about the power stage layout of the traction inverter.

Keywords: EV, powertrain, inverter, traction control, vehicle performance, powertrain

1 Introduction

The possibility to drive an electric vehicle with more than one motor has been widely investigated in the past 20 years [1]. There are three main reasons for having more than one traction motor: the power rating reduction of the electric drive with possible simplification and cost reduction of the power converter; the additional degree of freedom in vehicle torque vectoring for enhancing traction and stability control [2]; the increased reliability of the overall traction system [3].
Proposed solutions range from the simple single-motor drives coupled to one axle through a reduction differential gearbox, to the very complex solution of four direct drive motors integrated in the hub wheels, sharing the limited room with the brake disk, caliper and wheel suspension [4].

This work refers to the two-motor two-axle configuration for a compact car, shown in Figure1. This solution, using two-electric motors and two reduction differential gearboxes, drives all the four wheels of the vehicle. Front and rear motor drives are supplied by two different battery packs.
By using two-motor, two-axle configuration it is possible to choose different power and torque sizing for the drives and also to adopt different gear ratio for the gearboxes. The use of two traction drives improves the total tractive effort delivery in the whole speed range with respect to a single drive of the same total power rating. Section 2 gives a design method at equal cost and it is based on the evaluation of different performances at low, medium and high vehicle speed.

Figure 1 Picture of the AMBER-ULV car

Split of traction power between front and rear drives allows to reduce both traction drives power ratings. As a consequence of reduced power, it is possible to adopt even very low voltage values of the battery packs.

.

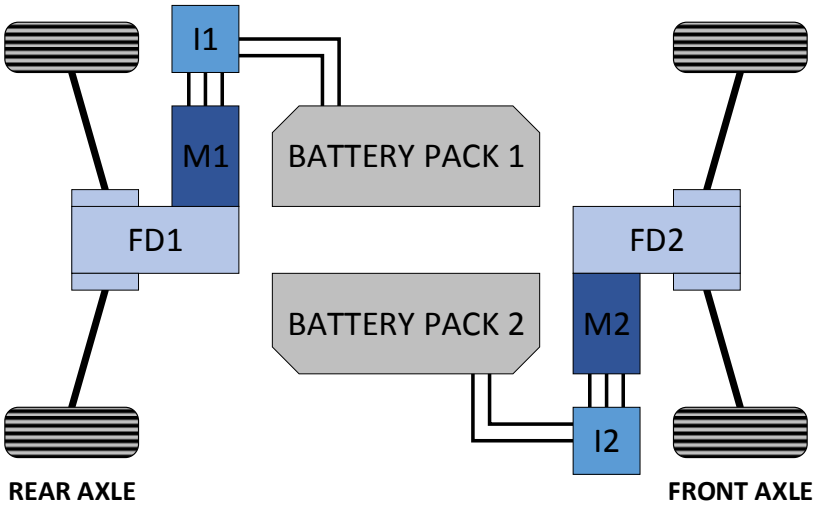

Figure 2 Powertrain configuration based on two-motor, two-battery and two-axle

Nowadays, active components at very low voltage (for example 75 V) are readily available, and development of inverters up to 40kVA (peak) at a DC-link voltage of 48 V are technically and economically feasible.
The use of low voltage level yields to reduced the insulation level for active components and to lower the electromagnetic emissions than higher voltage systems. The main reduction in system cost is than due to reduced utilization or no-utilization of shielded power cables and shielded component boxes, and to the use of simpler and cheaper connection systems. Low voltage systems are also well accepted by car manufacturers, services and final users for its intrinsic electric safety.
Decreasing the voltage level for the single battery pack yields to reducing cell unbalance issues and to minimizing the complexity of the equalization system. Lowering the number of cells connected in series to about 16 cells allows the use of low-cost lithium-ion cells with high dispersion of cell internal parameters. Nowadays, these ‘poor’ cells cannot be used on higher voltage systems without introducing expensive Battery Management System (BMS) with powerful equalization systems.
Section 3 gives a technical and economical comparison among several active components in the DC-link voltage range from 50 to 140V. Section 4 gives details about the layout design of a 15kVA (rated) current inverter power stage suitable to be used in the low and extra low voltage range.

The use of two drive systems for the traction of an electric vehicle introduces many control issues in the energetic, traction and stability management of the vehicle. A dedicated traction control system is still under development and it is not addressed in this paper.

The proposed powertrain was developed within the EU AMBER-ULV project. This project aims to develop a compact lightweight electric car with high driving performance and long range, suitable to be introduced into the market at affordable price in a small-medium production volume. Table 1 introduces the main technical specification of the AMBER-ULV car.

Table I Main AMBER-ULV car parameters

Curb mass	900 [kg]
4 passengers + payload	300 [kg]
Frontal section	2 [m^2]
Drag coefficient	0.33
Rolling resistance coefficient	0.016

2. Traction motor selection

This section reports the procedure adopted for front and rear motor selection. It aims to find the front-rear motor combination yielding to the best vehicle performance in the whole operating speed range of the vehicle. This section also presents an analytical method for defining the vehicle performance.
For the motor design, the mechanical constrains are given in Table 2. Electrical constrains are given in Table 3 for different values of the DC-link voltage, corresponding to the different battery pack arrangements that will be analyzed in Section 3. Mechanical constrains include size and speed limits while electrical ones are mainly related to the VA rating of the battery-inverter supply. Other motor technology related limits are given in Table 4.

Table 2 Main mechanical constrain on traction motors

Description	Value
Maximum overall motor length including coupling flange in the front and speed sensor on the rear	300 [mm]
Maximum external motor diameter, including cooling fin	210 [mm]
Maximum motor weight	40 [kg]
Cooling	natural air ventilation, transverse air direction
Maximum input speed of the reducer-differential gear-set	8000 [rpm]
Maximum input torque of the reducer-differential gear-set	140 [Nm]
Available reduction gear ratios	1:6.24; 1:7.16

Table 3 Electrical data of the inverter supply for different DC voltage ratings

Description	unit	Values				
Component break-down voltage	[V]	75	100	120	150	200
Approx. number of Ion-lithium cells		16	20	24	32	40
Approx. rated DC-link voltage	[V]	52	67	80	105	140
Minimum line-to-line voltage for obtaining the rated motor performance	[V_{RMS}]	33	42	52	67	84
Maximum rated current from the inverter	[A_{RMS}]	260	210	170	130	105
Maximum overload current from the inverter for 240 s	[A_{RMS}]	520	420	340	260	210
Maximum overload current from the inverter for 60 s	[A_{RMS}]	700	560	450	340	280
Maximum battery power	[kW]			27		

Table 4 Main technological constrains on traction motors

Description	Value
Motor technology	Induction, copper cage
Maximum magnetic sheet thickness	0.5 [mm]
Maximum specific power losses @1.5T	2.70 [W/kg]
Minimum air gap thickness	0.5 [mm]
Winding technology	Single layer winding
Number of pole	4
Maximum estimated motor cost for 100 units, fully manufactured in EU	€ 450

Table 5 Main performance of the two boundary motor solutions for: V_{LL}=65 [V_{RMS}]; I_{RATED}=135 [A_{RMS}]; I_{OVL}=340 [A_{RMS}]

		Motor P1 (high speed)	Motor P2 (high torque)
Rated torque T_{BASE}	[Nm]	21	34
Rated speed n_{BASE}	[rpm]	4000	2400
Constant power at I=I_{RATED}	[W]	10800	~10500
Constant power speed range I=I_{RATED}	[rpm]	~5500-7000	~3500-5200
Power at 7000rpm, I=I_{RATED}	[W]	10800	9800
Max torque at I=I_{OVL}	[Nm]	70	116
Max power at I=I_{OVL}	[W]	26000	24000
Speed of max power at I=I_{OVL}	[rpm]	3600	2150
Max power at n=7000 [rpm]	[W]	16000	9800

The application of all these constrains on the motor design procedure leads to seven theoretical possibilities of motors, all having the same external size, same weight and same rated power, but different mechanical output characteristic. Table 5 gives the main performance data for the two boundary motors, called high speed (P1) and high torque (P2) motor respectively. Figure 3 shows the maximum torque and power output of all the seven possible motors.

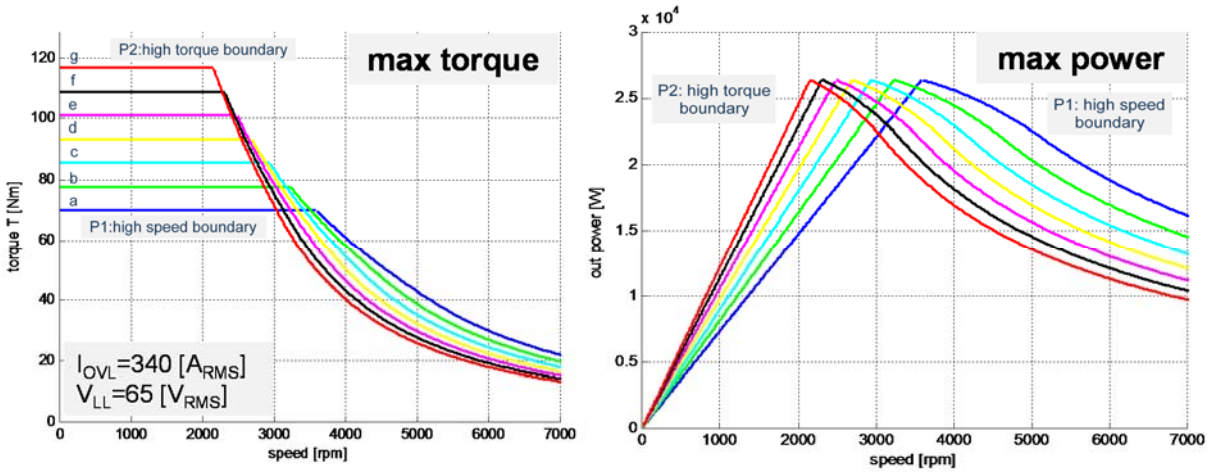

Figure 3 Limit mechanical output characteristics of possible motor designs

The dynamic performances of the car are numerically evaluated considering the tractive effort produced by the combination of the seven possible motors and the two possible gear ratios. In this analysis:

- Only the longitudinal acceleration is analyzed. Stability or traction control issues are not considered. Consequently, the vehicle performances are independent by the front/rear installation of the two motor-transmission combination.
- Only two combinations of gear ratios are detailed analyzed: (1:6.24 and 1:6.24), (1:6.24 and 1:7.16). The possible third one (1:7.16 and 1:7.16) is not shown in detail, because of evident lack of performance at high speed, with all the possible motor combinations. In total, 56 combinations have been computed and compared.

The main evaluation criteria for the selection of the best motor-transmission is based on the analysis of the total mechanical characteristic produced by the entire powertrain. The total mechanical characteristic is evaluated by introducing the four following indexes:

- **Maximum tractive effort at zero and low speed.** It defines the vehicle climbing capability. It also defines the initial vehicle acceleration. A minimum value is required for complying with the homologation standard (overcome uphill test).
- **Maximum power.** It is associated to the acceleration performance in medium-high range vehicle speed. It is usually obtained at a speed range of 50-60 km/h.
- **Power available at 40 km/h**. It defines the acceleration performance at low speed. The higher the power, the faster the acceleration at low-medium speed.
- **Power available at max speed**. It defines the capability of the vehicle to reach the maximum vehicle speed of 120 km/h, and the acceleration performance at high speed. A minimum value is requested in order to reach the expected maximum.

Each index is associated to the scoring table given in Table 6, representing a numerical evaluation of the vehicle performance. Scores have been assigned in the range 0-4 (0: not acceptable; 4: beyond expectation) by analyzing the dynamic performance of the AMBER-ULV car using a numerical model. Main car parameters are given in Table 1. The score assignments are based on benchmark analysis with similar vehicles and on analysis of performance expectation of potential drivers.

Table 6 Scoring of the four main vehicle dynamic maximum performances

Score	description	traction force at low speed [N]	max power [kW]	max power at 40 km/h [kW]	power at max speed [kW]
0	Unacceptable	<2800	<35	<25	<20
1	Acceptable	2800 to 3000	35 to 38	25 to 30	20 to 24
2	Less than average	3000 to 3300	38 to 41	30 to 35	24 to 26
3	Average	3300 to 3600	42 to 45	35 to 40	26 to 28
4	Good	3600 to 3900	45 to 48	40 to 45	28 to 30
5	Very good	>3900	>48	>45	>30

Figure 4 reports the scores obtained with the two combinations of gear ratios: (1:6.24 1:6.24) on the left, and (1:6.24 1:7.16) on the right. It also underlines that the selected optimal solution is the number 6 on the left column. This solution, with the same gear ratio (1:6.24) for both axles, is preferred to solutions with higher total score because of good performance (score of 4) in all the four indexes. It corresponds to good performances in the whole speed range of the vehicle.
Figure 5 gives the mechanical output in terms of tractive effort and power of the chosen solution. It also shows that the two power peaks generated by the two drives occur at different vehicle speeds. This feature implies a high power outcome for a wide speed range. The resulting max power curve is the key factor for obtaining high performance at medium-high vehicle speed. This power characteristic represents one of the main advantages between the proposed dual-motor powertrain configuration and a standard single-motor solution.

Performance selection table for the two traction motors. front gear ratio: 1:6.24; rear gear ratio: 1:6.24							
n.	Rear motor	Front motor	Low speed tractive effort	Max power	Power at 40 km/h	Power at max speed	Total score
1	a	a	1	5	2	5	13
2	a	b	2	5	2	5	14
3	a	c	2	5	3	5	15
4	a	d	3	4	3	5	15
5	a	e	3	4	3	5	15
6	a	f	4	4	4	4	16
7	a	g	4	4	4	3	15
8	b	b	2	5	3	5	15
9	b	c	3	5	3	5	16
10	b	d	3	5	3	4	15
11	b	e	3	4	4	3	14
12	b	f	4	4	4	3	15
13	b	g	4	4	4	3	15
14	c	c	3	5	3	3	14
15	c	d	3	5	4	3	15
16	c	e	4	5	4	3	16
17	c	f	5	5	4	2	16
18	c	g	5	4	5	2	16
19	d	d	4	5	4	2	15
20	d	e	5	5	4	2	16
21	d	f	5	5	5	2	17
22	d	g	5	5	5	2	17
23	e	e	5	5	5	2	17
24	e	f	5	5	5	1	16
25	e	g	5	5	5	1	16
26	f	f	5	5	5	1	16
27	f	g	5	5	5	1	16
28	g	g	5	5	5	1	16

Performance selection table for the two traction motors. Front gear ratio: 1:6; rear gear ratio: 1:7.16							
n.	Rear motor	Front motor	Low speed tractive effort	Max power	Power at 40km/h	Power at max speed	Total score
1	a	a	2	5	2	4	13
2	a	b	2	5	3	4	14
3	a	c	3	5	3	4	15
4	a	d	4	5	3	3	15
5	a	e	4	5	4	3	16
6	a	f	5	5	4	2	16
7	a	g	5	5	4	2	16
8	b	b	3	5	3	3	14
9	b	c	3	5	4	3	15
10	b	d	4	5	4	3	16
11	b	e	5	5	4	2	16
12	b	f	5	5	5	2	17
13	b	g	5	5	5	2	17
14	c	c	4	5	4	2	15
15	c	d	5	5	4	2	16
16	c	e	5	5	5	1	16
17	c	f	5	5	5	1	16
18	c	g	5	5	5	1	16
19	d	d	5	5	5	2	17
20	d	e	5	5	5	2	17
21	d	f	5	5	5	1	16
22	d	g	5	5	5	1	16
23	e	e	5	5	5	1	16
24	e	f	5	5	5	1	16
25	e	g	5	5	5	1	16
26	f	f	5	5	5	1	16
27	f	g	5	5	5	1	16
28	g	g	5	5	5	0	15

Figure 4 Scores obtained with two combination of motor and gear ratio

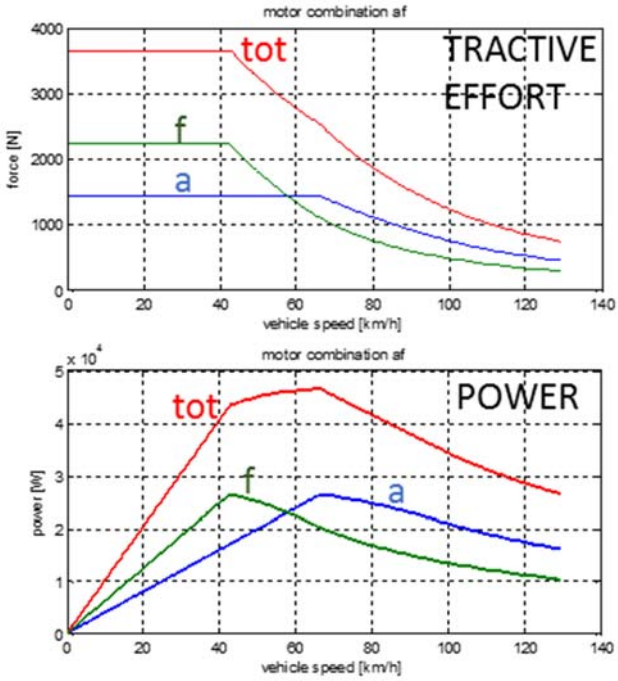

Figure 5 Tractive effort and power for the chosen combination

The selected combination (Figure 4, left column, n.6) has been numerically verified on several real urban and extra-urban driving cycles. The diagrams of Figure 6 demonstrate the capability of the proposed configuration to follow the 'Artemis rural' driving cycle.

Figure 6-a and Figure 6-c give the total generated tractive effort compared with the available force from the traction system, which is the sum of the two efforts produced by the two separate drives. Output force and limits for the two separate drive drives are also given in Figure 6-b and 6-c. The analysis of the diagrams of Figure 6 clearly shows that the proposed powertrain satisfies all the dynamic requirements of the 'Artemis rural' driving cycle. Moreover, the results demonstrate that the braking capability of the electric powertrain is potentially able to produce the required braking force in 99% of braking operation.

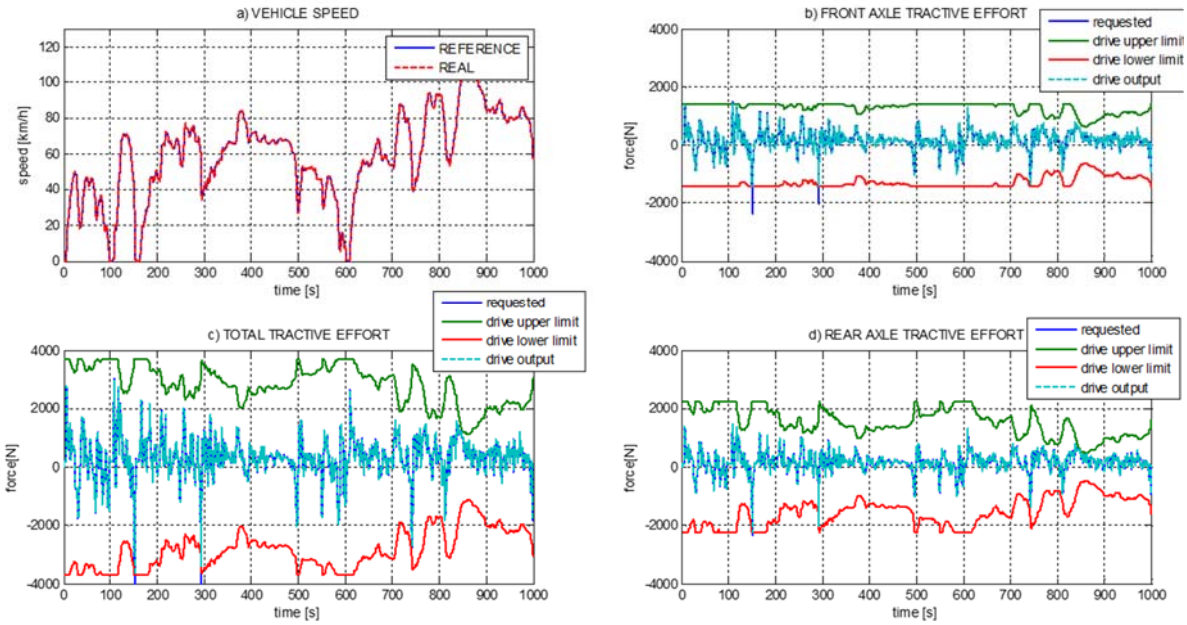

Figure 6 Artemis-rural driving cycle. Speed profile and tractive effort for combination a and f, gear ratio 6.14 for both axles.

The estimated dynamic performance of the selected solution (motor a and f, gear ratio 6.14 for both axles) is summarized in Table 7.

Table 7 Calculated dynamic performance for the selected motor/transmission combination

PERFORMANCE	VALUE	UNIT
acceleration 0 to 10 km/h	0.9	[s]
acceleration 0 to 50 km/h	4.7	[s]
acceleration 0 to 70 km/h	7.1	[s]
acceleration 0 to 100 km/h	13.4	[s]
max. speed	~130	[km/h]
time 0 to 50 m	5.7	[s]
time 0 to 100 m	8.4	[s]
time 0 to 1000 m	37	[s]

3 Inverter active component selection

A key point for the optimal design of an electric powertrain is the choice of the battery pack voltage and the resulting voltage rating of the inverter.
This Section investigates the possibility of realizing the inverter for the two motors selected in Section 2 using low and extra-low voltage solutions. A comparison among different available components and mounting technologies is presented. A layout is also proposed for testing different technologies.
Figure 7 compares the power-cost density of active components suitable to be used for the power stage of a three-phase traction inverter. This preliminary comparison does not take into account the mounting and assembling cost. As it is widely known, IGBTs are preferred when working at higher voltage, while MOSFETs are preferred at lower voltage. This first analysis indicates that it is possible to find MOSFET and IGBT with similar power-cost density and that actual MOSFET technology reaches its optimal power-cost density at lower voltage levels. Since the use of very high voltage is out of the scope of this study for the induced cost of battery pack, power wiring harness and EM shields, the comparison has been focused on MOSFET technology. Figure 8 shows the single MOSFET performance in terms of theoretical converted power vs. lost power. From this point of view, it is possible to find MOSFETs with very similar performance for almost all the voltage range.

From the single MOSFET analysis, it is possible to switch to the three-phase inverter design by assuming a target power output of 15kVA. This power rating complies with the supply requirements of the two motors selected in Section 2. The rated battery voltage considered in this analysis ranges between 50 and 130V. Table 3 gives the corresponding electrical characteristic of five possible inverters in rated and overload condition.

For each solution, starting from the MOSFET characteristic, it is possible to choose the right number of MOSFETs to connect in parallel. An even number of parallel MOSFET is necessary due to layout optimization. Table 8 gives the main MOSFET characteristics for every considered type. Table 9 shows the number of MOSFETs in parallel required to obtain the performance demanded in Table 3 and the resulting real performance of the inverter.

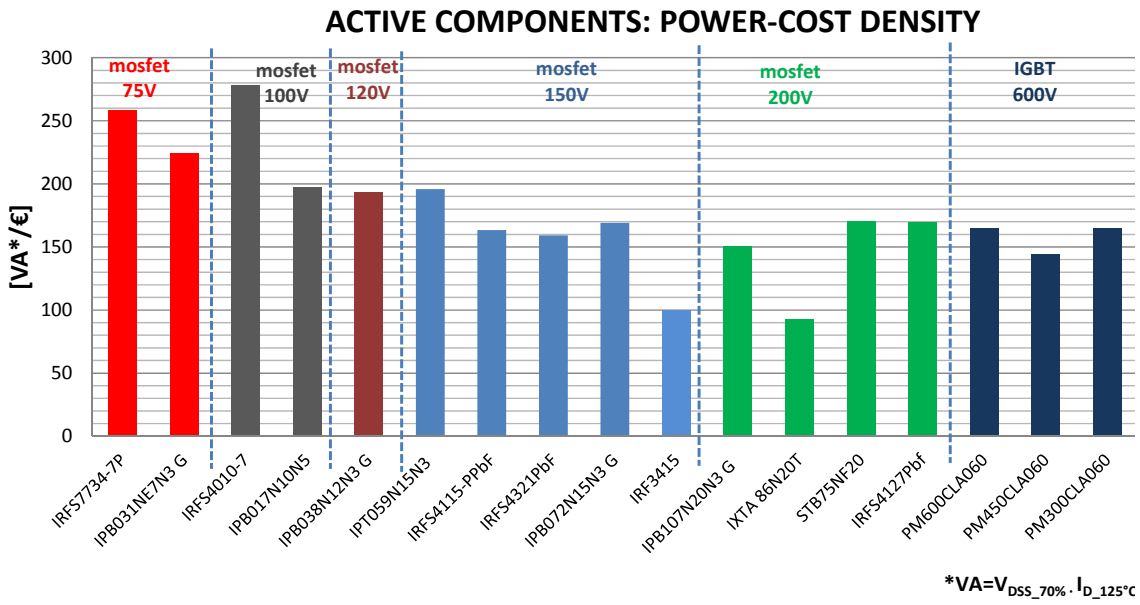

Figure 7 Power-cost density for commercially available power active components suitable for the power stage of traction inverter

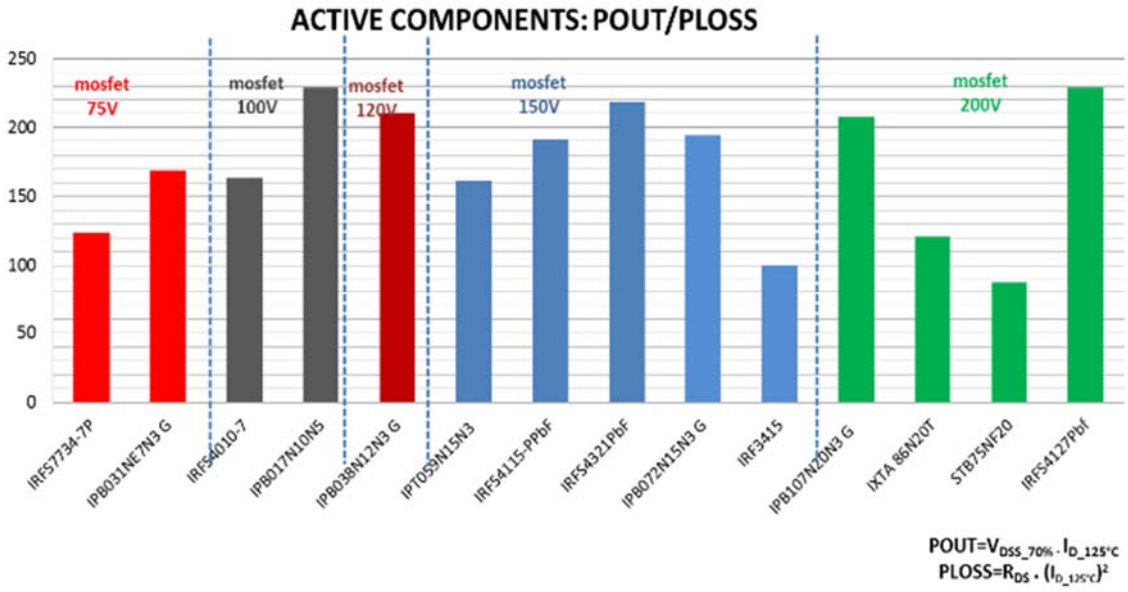

Figure 8 Performance factor of commercially available MOSFETS suitable for realizing the power stage of traction inverter

Table 8. Main characteristics of the considered active components (MOSFETs)

n.	Name	Manufacturer	package	I_d 125°C [A]	Breakdown voltage V_{BRDS} [V]	reference battery voltage [V]	R_{DSON} [mΩ]
1	IRFS7734-7P	IR	D2Pack-7pin	139	75	52	3.05
2	IPB031NE7N3 G	INFINEON	D2Pack	100	75	52	3.10
3	IRFS4010-7	IR	D2Pack-7pin	130	100	67	3.30
4	IPB017N10N5	INFINEON	D2Pack-7pin	180	100	67	1.70
5	IPB038N12N3 G	INFINEON	D2Pack	105	120	80	3.80
7	IPT059N15N3	INFINEON	HSOF-8	110	150	105	5.90
8	IRFS4115-PPbF	IR	D2Pack	55	150	105	10.00
9	IRFS4321PbF	IR	D2Pack	40	150	105	12.00
10	IPB072N15N3 G	INFINEON	D2Pack	75	150	105	7.20
11	IRF3415	IR	D2Pack	25	150	105	42.00
12	IPB107N20N3 G	INFINEON	D2Pack	63	200	140	10.70
13	IXTA 86N20T	IXIS	D2Pack	40	200	140	29.00
14	STB75NF20	ST	D2Pack	47	200	140	34.00
15	IRFS4127Pbf	IR	D2Pack	51	200	140	12.00

Table 9 Main parameters and performance for possible inverter configuration

n.	Name	V_{BRDS} [V]	MOSFET in parallel	Equivalent R_{DS} [mΩ]	Output rated current [A_{RMS}]	Output maximum current [A_{RMS}]	Nominal power [VA]	Maximum power [VA]
1	IRFS7734-7P	75	6	0.51	237	710	15240	45721
2	IPB031NE7N3 G	75	8	0.39	227	681	14619	43857
3	IRFS4010-7	100	4	0.83	148	443	12670	38009
4	IPB017N10N5	100	4	0.43	204	613	17543	52628
5	IPB038N12N3 G	120	6	0.63	179	536	18420	55260
7	IPT059N15N3	150	4	1.48	125	374	16081	48243
8	IRFS4115-PPbF	150	8	1.25	125	374	16081	48243
9	IRFS4321PbF	150	12	1.00	136	409	17543	52628
10	IPB072N15N3 G	150	6	1.20	128	383	16446	49339
11	IRF3415	150	16	2.63	113	340	14619	43857
12	IPB107N20N3 G	200	6	1.78	107	322	18420	55260
13	IXTA 86N20T	200	8	3.63	91	272	15594	46781
14	STB75NF20	200	6	5.67	80	240	13742	41226
15	IRFS4127Pbf	200	6	2.00	87	260	14911	44734

For any inverter configuration, Figure 9 and Figure 10 represent conduction power losses for output powers of 15kVA (rated condition) and 35kVA (overload condition) respectively.

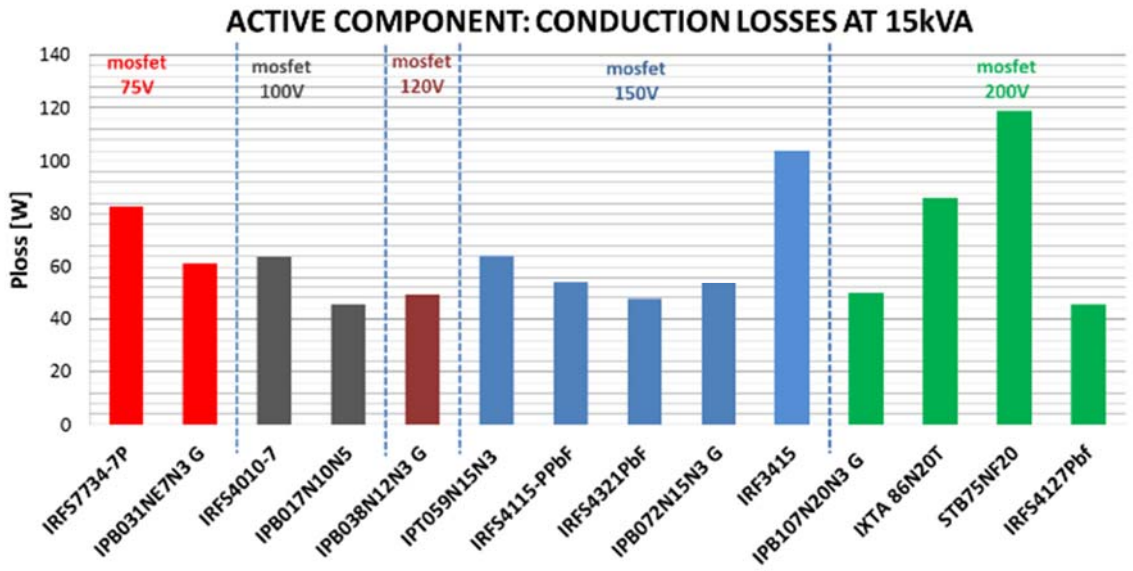

Figure 9 Conduction losses of three-phase traction inverters realized with different MOSFETs at 15kVA (rated condition)

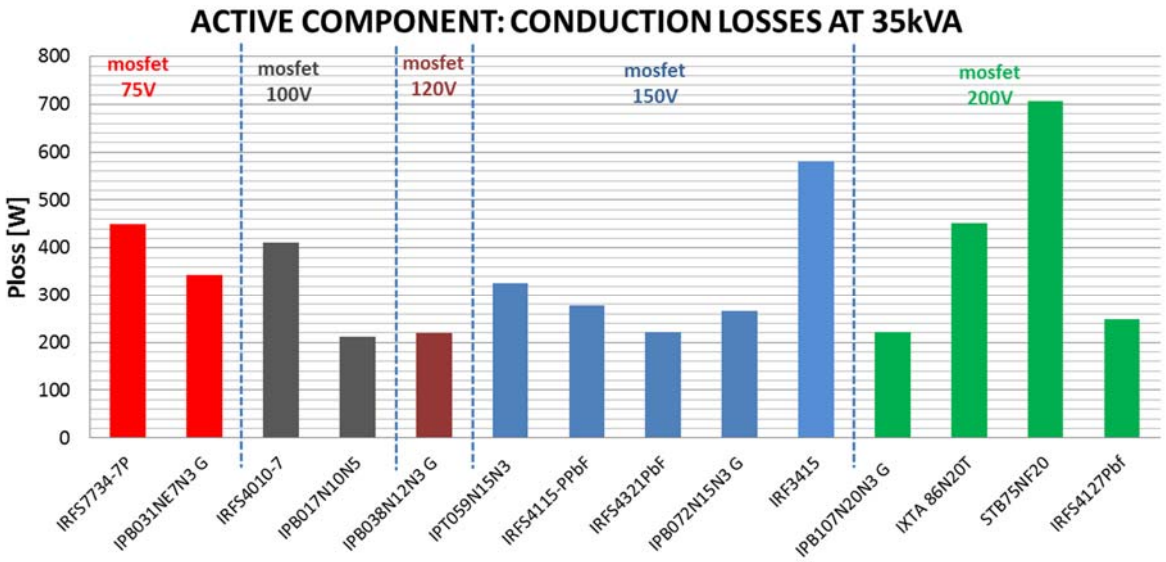

Figure 10 Conduction losses of three-phase traction inverters realized with different MOSFETs at 35kVA (overload condition)

The cost of the active components roughly represents 30% to 50% of the cost of the power stage of the inverter. The higher the current, the higher the cost of the power circuit and then the lower the percentage of the active components cost. Recent improvement in mounting technologies (IMS, DBC and Thick copper PCB) contribute lowering the cost of the power circuitry even for very high current output.
The cost of the DC-link capacitors is mainly associated to the kVA rating, but a certain dependency can be found to the DC-link voltage. For example, the cost for the 200V voltage rating, the cost is increased due to lack of suppliers. For this reason, inverter cost comparison is performed taking into account only the active components. Resulting components cost for each inverter is given in Figure 11.

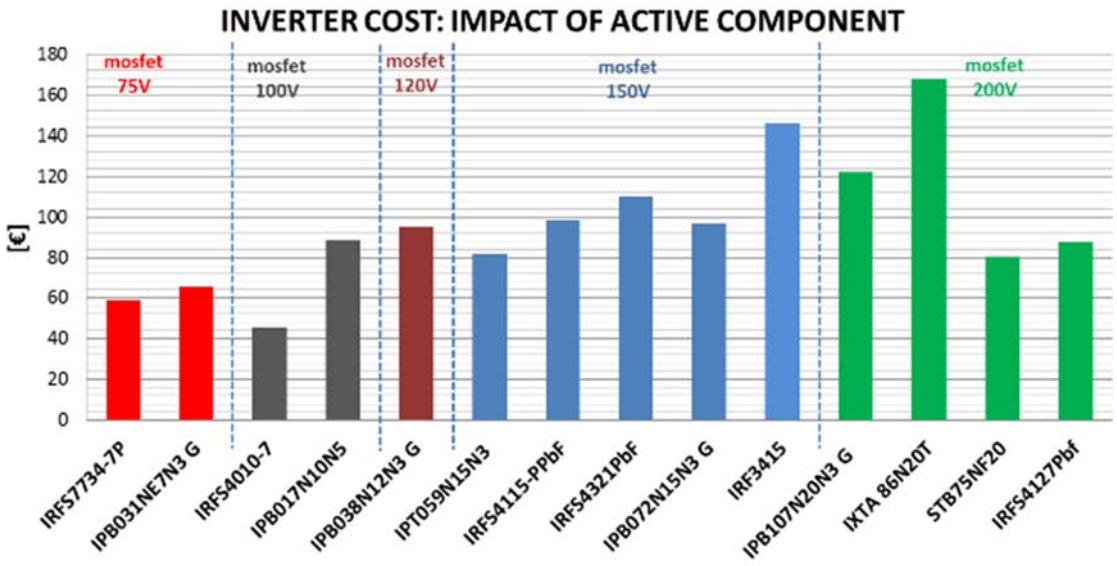

Figure 11 Component costs for a 15kVA three-phase traction inverter with different MOSFETS

Results obtained with the different solutions can be summarized as follows:

- All the voltage range V_{BRDS}=75÷200V can be used for the selected application. It means a battery pack composed of 16 to 42 cells connected in series.
- Number of MOSFET in parallel ranging from 4 to 16. A number larger than 12 should be avoided in order to keep the complexity of the power circuits below acceptable levels. The larger the number of power MOSFET in parallel, the wider the planar footprint of the inverter power stage will be.
- Voltage level V_{BRDS}=120V has only one supplier. For this reason, at the moment, it is suggested to avoid it.
- Losses are minimized for the 100V and 150V rating. The lower the conduction losses, the simpler the design of the cooling system.
- Voltage level V_{BRDS}=100V has the best results in terms of cost. It is worth noting that the best solution at V_{BRDS}=150V has a cost of active component 60% higher than the best solution at V_{BRDS}=100V.

A first conclusion of this analysis is that the MOSFETs in the voltage classes V_{BRDS}=150V and 100V represent the two best options, at the moment, for realizing an automotive inverter with a rated power of approximately 15kVA and a maximum power of at least 35kVA.
A second conclusion is the demonstration of the technical and economic feasibility of very low voltage system for the power range under investigation. From this analysis, the design of the two traction inverters using MOSFETs at V_{BRDS}=75V for the DC-link voltage of about 48-53V (16 ion-lithium cells) is fully justified.

4. Inverter layout

The main feature of the adopted inverter layout is being able to compare two different mounting technologies for the active component: the Insulated Metal Substrate (IMS) and the Direct Bond Copper (DBC) substrate. This accomplishment is achieved using:

- one main board, based on standard FR4 PCB with 6 copper layer 100µm thick, containing the DC capacitor, DC power connections and driver circuits.
- three identical power modules for the three phase legs, that can be realized either in DBC or IMS technology.

The idea is to create a common layout for the main board which is able to host different solution for the power modules. In this way, assembly, testing and evaluation can be done using the same boundary condition for the power modules.
Figure 12 represents the basic coupling principle between the DC-link main board and a power module board. This solution allows the power module board to be made using the selected technology (IMS or DBC) and to install it inside the DC-link board. This assembly must be created using a standard mounting process.

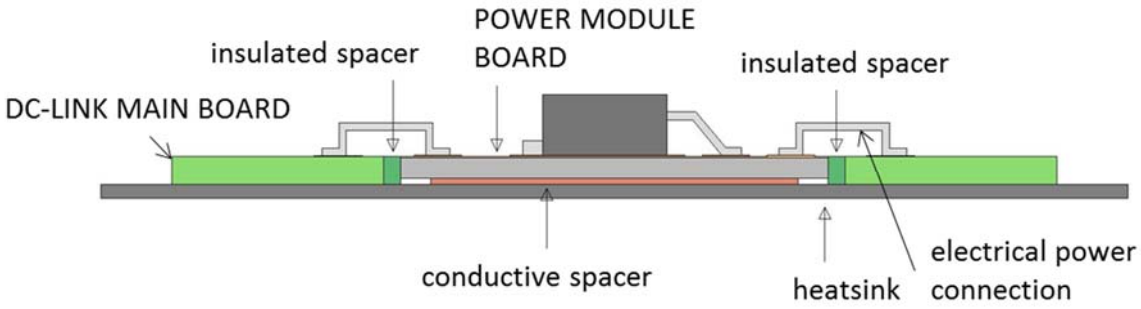

Figure 12 Mechanical integration of a power module within the DC-link board

In order to host the three power modules, the DC-link board is constructed as shown in Figure 13 and Figure 14. As revealed in these two figures, the structure of the DC-link main board has the following properties:

- The board hosts the DC capacitors, the driver circuit and all the DC-link power connections
- The three holes can accommodate three power modules. The power module technology does not interfere with the DC-link board design and mounting process.
- The electrical connection between the power module and the DC-link board is obtained using surface mount power jumpers soldered on both side.

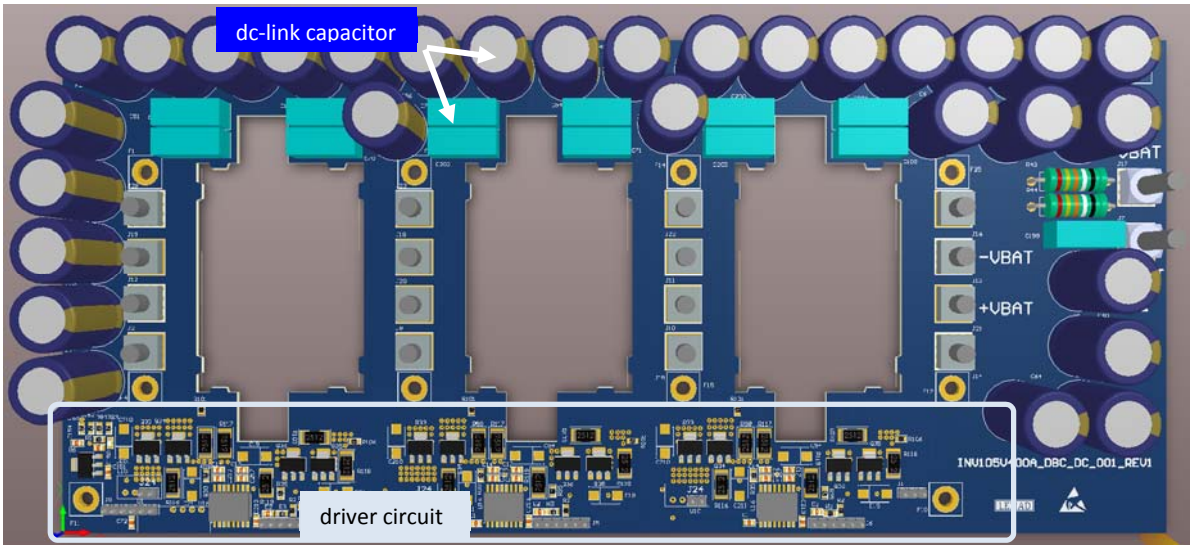

Figure 13. DC-link main board. Top view

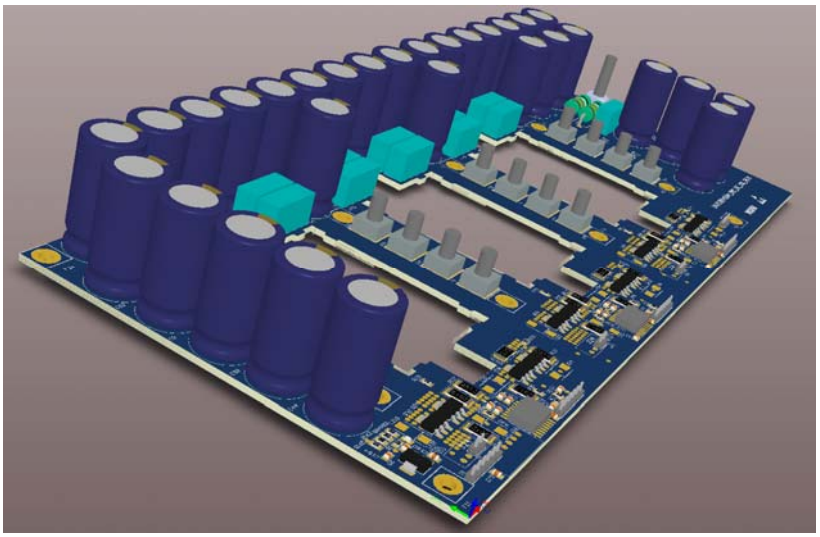

Figure 14 DC-link main board. Side view

The layout design of the power module has been optimized for its insertion in the hole of the DC-link board. In particular, it allows the use of the same circuit layout, mounting technology and power electrical connection with the DC-link board regardless of the board technology (IMS or DBC) used. Figure 15 shows the proposed solution for the circuit layout of the power module. In this solution, all the connection between the DC-link and the power module are obtained by using surface mount jumpers. Jumpers create the connection for:

- DC link positive polarity
- DC link negative polarity
- Output phase
- Gate signal
- Temperature sensor

The main feature of this solution is the possibility of fully automate the mounting process of the power modules inside the DC-link board using standard pick-and-place machines.

Figure 16, finally shows a picture of the developed inverter with the power modules mounted inside the main DC-link board. The main specifications and characteristics of the proposed inverter are given in Table 10.

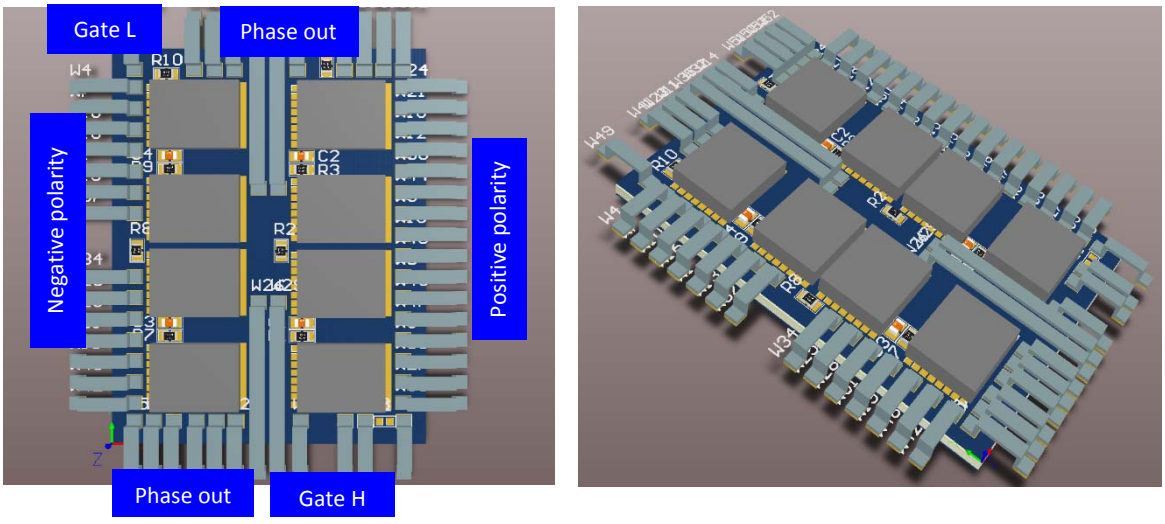

Figure 15 Power module. Top and side view view of the assembly.

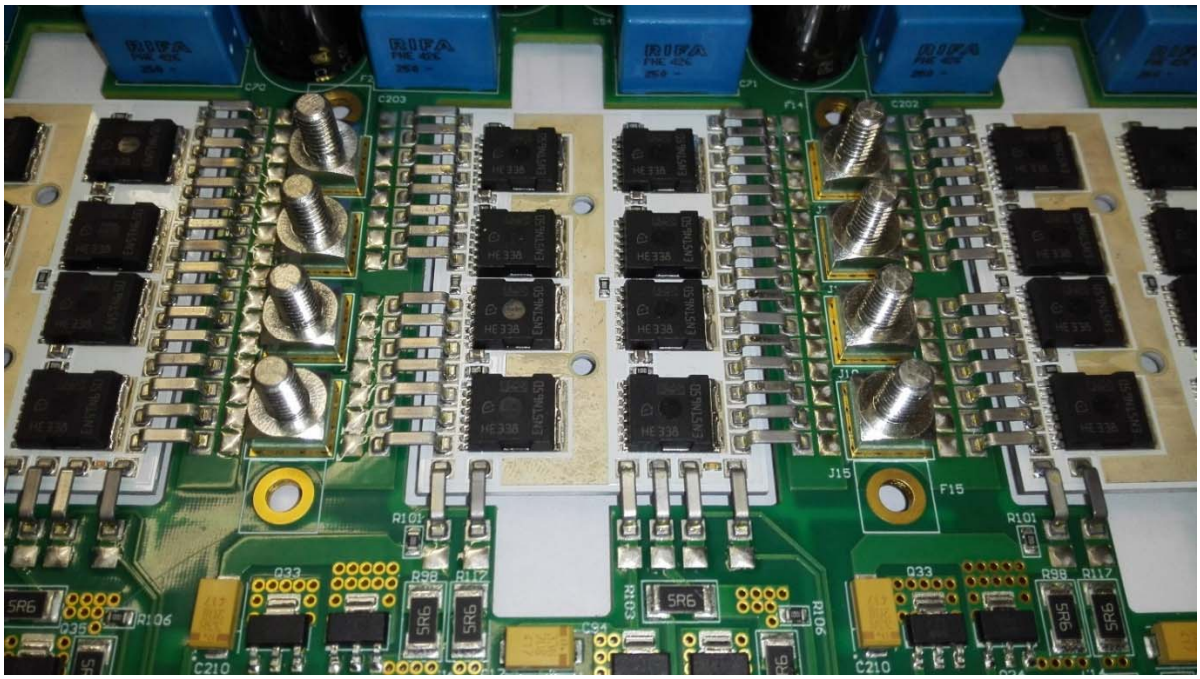

Figure 16 View of the complete assembly of the DC-link and power module

Table 10 Main specification of the designed traction inverters

PARAMETER	VALUE	UNIT
MOSFET type	Infineon IPT059N15N3	
Equivalent R_{DS}	1.48	[mΩ]
Number of MOSFET in parallel	4	
Gate resistance	10	[Ω]
Gate additional external capacitance	100	[pF]
Rated DC-link voltage	100	[V]
Breakdown voltage components	150	[V]
Rated thermal output current	135	[A_{RMS}]
Maximum output current 120 s	350	[A_{RMS}]
Maximum output current 420s	270	[A_{RMS}]
Output nominal power (at 135A)	15	[kVA]
Output maximum power (at 350A)	40	[kVA]
Switching frequency	7.5	[kHz]
Max dimension (of power stage)	300x150	[mm]
Heatsink cooling	Air	
Heatsink nominal thermal resistance	0.40	[°C/W]
Maximum operating die temperature	125	[°C]
Absolute maximum die temperature	175	[°C]
Power stage temperature sensor	One sensor per leg	
Driver circuit type	Push pull amplifier	
Peak driver circuit output current	20	[A]

4 Conclusion

A two-motor, two-axle solution has been proposed for the traction system of a full performance compact car (AMBER-ULV project). The paper introduces a method for selecting the optimal front-rear motor-transmission combination that provides the best driving performance under a set of mechanical and electrical constrains. Splitting the traction power between two drives makes it feasible for a low voltage solution. This possibility is investigated in the range from 50 to 140V, under both a performance and an economical point of view. Finally, a layout for the inverter power stage is proposed. This layout has the unique feature of being used for testing two different mounting technologies: IMS and DBC.
A dedicated traction control system is under development for this powertrain and it will be presented in future papers together with vehicle road test results. The main task of the traction control system is the generation of the two torque references for the two motor drives by taking into account the driver commands, the limitations coming from the drives, the limitations from the battery packs and power sharing between the two drives. Additionally, the traction control system is able to manage the powertrain in degraded operating conditions and to follow the torque references generated by the active stability control system.

Acknowledge

FP7 European Union project

Topic	GC.SST.2013-3 - Future light urban electric vehicle
Project Number	604766
Project Acronym	AMBER-ULV
Project title	Automotive Mechatronic Baseline for Electric Resilient Ultra-Light Vehicle

References

[1] Jager, B.; Neugebauer, P.; Kriesten, R.; Parspour, N.; Gutenkunst, C., “Torque-vectoring stability control of a four wheel drive electric vehicle” in *IEEE IVS*, June-July 2015;
[2] Juyong K.; Jinho Y.; Kyongsu Y., “Driving Control Algorithm for Maneuverability, Lateral Stability, and Rollover Prevention of 4WD Electric Vehicles With Independently Driven Front and Rear Wheels” in *IEEE TVT*, 60(7):2987-3001, Sept. 2011;
[3] Negarestani, S.; Ghahnavieh, A.R.; Mobarakeh, A.S., “A study of the reliability of various types of the electric vehicles” in *IEEE IEVC*, March 2012;
[4] Jae-Han S.; Byeong-Hwa L.; Young-Hoon J.; Jung-Pyo H., “Optimum design of IPMSM for in-wheel direct-drive by response surface methodology and FEA”, in *IEEE EVS27*, Nov. 2013;
[5] De Novellis, L.; Sorniotti, A.; Gruber, P., “Wheel Torque Distribution Criteria for Electric Vehicles With Torque-Vectoring Differentials” in *IEEE TVT*, 63(4):1593-1602, May 2014.